Titanium-iridium oxide layer coating to suppress photocorrosion during photocatalytic water splitting

Yongwoo Kwon and Hyunjoo Lee[†]

Department of Chemical and Biomolecular Engineering, Korea Advanced Institute of Science and Technology,
Daejeon 305-701, Korea

Abstract−Photocatalysts with a small band gap energy have received a great deal of interest due their high solar conversion efficiencies. Cuprous oxide (Cu_2O) has attracted attention because of its small bandgap energy, a direct bandgap structure, its suitable band structure for water splitting, high absorption coefficient, non-toxicity, and its large abundance. However, it has poor stability due to the fickle oxidation states of copper. To enhance the stability and the production rate of hydrogen and oxygen, a $TiIrO_X$ overlayer was successfully formed on the Cu_2O under various synthesis conditions. The composition and oxidation state of the Ir species in the overlayer were optimized through the control of the Ir precursor and the amount of water. The Ir/Ti precursor molar ratio was linearly related to the surface Ir/Ti molar ratio. The addition of water converted the Ir precursor to IrO_2. The thickness of the overlayer was controlled by differing the synthesis times of the coating. Then, the largest amounts of hydrogen and oxygen were produced through the optimization of the $TiIrO_X$ overlayer with a higher IrO_2 fraction and a thicker overlayer.

Keywords: Photocorrosion, Water Splitting, Cuprous Oxide, Stability, $TiIrO_X$

INTRODUCTION

Photocatalytic water splitting has been studied to produce hydrogen with an environmentally friendly process [1,2]. Since Fujishima and Honda first reported the hydrogen evolution in a photoelectrochemical cell using an n-TiO_2 electrode [3], semiconductor-based photocatalytic water splitting has been studied as an important alternative for energy production [4-6]. Representatively, titanium oxide-based photocatalysts (e.g., TiO_2, $SrTiO_3$) have been studied in various reports [5,7-12]. However, these materials have absorbed an ultraviolet light because of their large bandgap energies (~3.2 eV). The solar conversion efficiency would be only 2% when UV light up to 400 nm is used. Therefore, splitting water under visible light has been an important but challenging goal [1].

During the water splitting reaction, stability is an important issue. Many photocatalysts that absorb visible light are photo-corroded under bandgap excitation [13-18]. For example, CdS is an excellent photocatalyst for the evolution of H_2 with visible light irradiation because of its small bandgap and suitable band position. However, sulfur in CdS, rather than H_2O, is oxidized by the photogenerated holes and is accompanied with the dissolution of cadmium [14,15].

Cuprous oxide (Cu_2O) is also a promising material for photocatalytic water splitting because of its direct small bandgap (~2.0 eV), a suitable band structure for water splitting [19-21], a high absorption coefficient [22], non-toxicity, and the abundance [23]. However, its poor stability in aqueous solutions and during the pho-

toreaction limits its application for the actual water splitting reaction [24-27]. Because the redox potentials of Cu_2O/Cu and Cu_2O/CuO are located between the conduction band and the valence band, the oxidation state of Cu_2O is easily changed by the photogenerated electrons and holes [22,27,28]. The photocorrosion causes the poor durability during the photocatalytic water splitting [25,27].

In our previous work, differently shaped Cu_2O colloidal particles were synthesized, and their stabilities in deionized water with or without light irradiation were tested [29]. All of the shaped Cu_2O particles had very poor stability. The Cu_2O particles were coated with a $TiIrO_X$ overlayer to enhance their stabilities and to suppress photocorrosion. The $TiIrO_X$ overlayer enabled the transfer of both electrons and holes. However, the coating did not completely prevent contact with water, which allowed for small degradation of the hydrogen/oxygen production. The $TiIrO_X$ overlayer should be optimized further to enhance the activity and stability.

In this work, a $TiIrO_X$ overlayer was coated onto colloidal Cu_2O particles ($TiIrO_X$/Cu_2O) by controlling various factors. The $TiIrO_X$/Cu_2O particles were used as photocatalysts for the overall water splitting. The $TiIrO_X$ overlayer was optimized by controlling the amounts of the iridium precursor, the amount of water added during the synthesis of the overlayer, and the synthesis time for the coating. The formation of IrO_2 in the coating overlayer was confirmed with X-ray photoelectron spectroscopy (XPS). The thickness of the overlayer and the formation of IrO_2 were important to enhance the H_2 and O_2 production rates.

MATERIALS AND METHODS

1. Materials

Copper (II) sulfate pentahydrate ($CuSO_4$·$5H_2O$, 98%), sodium

[†]To whom correspondence should be addressed.
E-mail: azhyun@kaist.ac.kr

hydroxide (NaOH, 97%), oleic acid (99%), D-(+)-glucose (99%), titanium butoxide (TBOT, 97%), iridium (III) chloride hydrate (IrCl$_3$·xH$_2$O, 99.9%), and anhydrous ethanol (EtOH, 99.5%) were purchased from Sigma Aldrich. Deionized water (18.3 MΩ cm) was purified by Human Power II+ Scholar (Human Corporation).

2. Synthesis of Cuprous Oxide

Cu$_2$O particles were synthesized through a previously reported method [30]. CuSO$_4$·5H$_2$O 1 mmol was dissolved in 40 ml of deionized water. Then, 6 ml of oleic acid was dissolved in 20 ml of ethanol, and this solution was added to the other solution under vigorous stirring to obtain Cu$_2$O particles. After the solution was heated to 100 °C, 10 ml of a 0.8 M NaOH aqueous solution was injected, and the mixture was kept at this temperature for 5 min. Subsequently, 3.42 g of D-(+)-glucose was dissolved in 30 ml of water and added to the previous solution, and the new solution was then stirred for 3 h. The final solution was washed with isopropyl alcohol and ethanol and collected by centrifugation. The collected particles were then dried at 50 °C for 3 h under a vacuum.

3. Coating Cuprous Oxides with TiIrO$_x$ Overlayers

TiIrO$_X$ overlayers were coated onto the Cu$_2$O particles. First, 33 mg of the Cu$_2$O particles was dispersed into 5.4 ml of anhydrous EtOH. Then, 3.8 mg of IrCl$_3$·xH$_2$O (0.95, 1.9, and 4.8 mg of IrCl$_3$·xH$_2$O were also used to examine the precursor effect) was dissolved in 5 ml of anhydrous EtOH, and 168 μl of water (120, 144, and 200 μl of water were also used to examine the water effect) was added to the above solution. Subsequently, 45 μl of TBOT was added into 5 ml of cold, anhydrous EtOH. Three solutions were kept at 0 °C and were mixed under vigorous stirring; they were maintained at the same temperature for 1 h (the times were also varied, and 0.5, 2, 3, and 5 h were utilized). The reddish solution was then washed with water and ethanol several times and then dried in a vacuum oven at 50 °C. The powder was heated at 210 °C for 2 h under nitrogen.

4. Hydrogen and Oxygen Production by Splitting Water

A 100 ml of quartz flask was used with a quartz plate window and a Teflon cover with two tubes. The tubes were connected to a gas chromatograph (GC) and an Ar cylinder. Each 0.1 g sample was dispersed into 100 ml of deionized water without a sacrificial agent. After Ar purging for ~20 min (until no nitrogen peak was detected by GC), irradiation was applied for 24 h. The light source was a 300 W Xe lamp, and the distance from the light source to the reactor was 20 cm with a 1-cm-thick water bath. After the reaction,

25 ml of Ar was injected into the reactor, and the outlet products were analyzed by a GC (Younglin GC 6000 series) that was equipped with a thermal conductivity detector (TCD).

5. Characterization

An X-ray photoelectron spectrometer (XPS; K-alpha, Thermo UK) equipped with a monochromatic Al Kα X-ray source (12 kV, 3 mA) was used to determine the surface properties of the nanoparticles. Binding energies were calculated by using the maximum intensity of the C 1s signal at 284.8 eV as a reference. The morphologies of the samples were investigated by field emission scanning electron microscopy (FE-SEM; JEOL6701, 5 kV) and transmission electron microscopy (TEM; Tecnai TF30 ST).

RESULTS AND DISCUSSION

When Cu$_2$O particles were used directly for water splitting, hydrogen initially appeared, but no oxygen was evolved. The holes generated upon light absorption were used for the oxidation of Cu$_2$O to CuO, so smooth Cu$_2$O surfaces turned into thorny CuO; photocorrosion occurred. Then photocatalytic water splitting stopped, and no more hydrogen was produced [29].

To protect Cu$_2$O from photocorrosion, titania-iridium oxide (TiIrO$_X$) overlayers were formed on the Cu$_2$O particles. TiO$_x$ would serve as electron pathways through which electrons generated inside Cu$_2$O semiconductor could be transported to the surface, and IrO$_2$ would serve as hole pathways through which holes could transfer to the surface. Fig. 1(a) clearly shows the rhombic dodecahedral shape of Cu$_2$O particles. After the TiIrO$_X$ coating, the coating layers were smoothly deposited onto the Cu$_2$O particles (Fig. 1(b)).

The chemical composition of the TiIrO$_X$ overlayers was investigated by EDX analysis. Fig. 2(a) depicts the TEM-HAADF image of the TiIrO$_x$-coated Cu$_2$O. Energy dispersive X-ray spectroscopy (EDX) data from the region marked as spot 1 in Fig. 2(a) are plotted and are displayed in Fig. 2(b), which clearly indicates the presence of Ti, Ir, Cu, and O. C and Cu signals in the EDX spectra were attributed to the carbon-coated copper grid. These results confirmed that the coated layers consisted of TiIrO$_X$.

To enhance the activity towards photocatalytic water splitting, the synthetic condition of the overlayers was optimized by controlling the Ir/Ti precursor ratio, the amount of water, and the synthesis time of the coating. Various Ir/Ti precursor ratios (5, 10, 20,
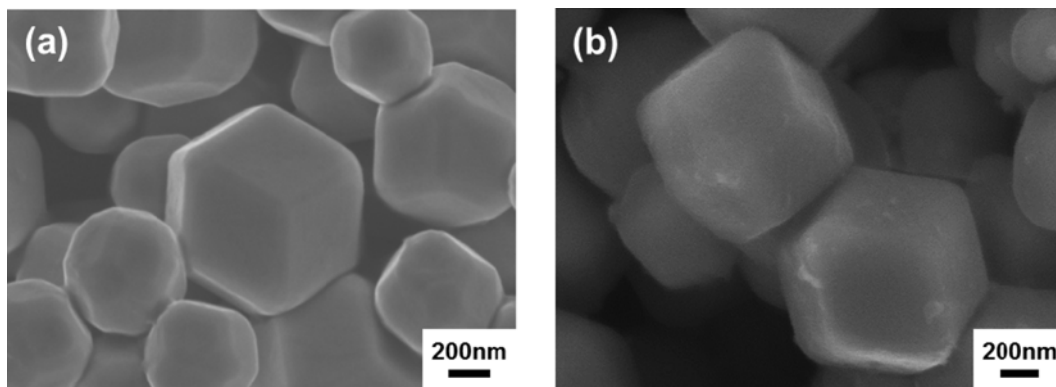

Fig. 1. SEM images of (a) bare rhombic dodecahedral Cu$_2$O and (b) TiIrO$_X$-coated rhombic dodecahedral Cu$_2$O particles.
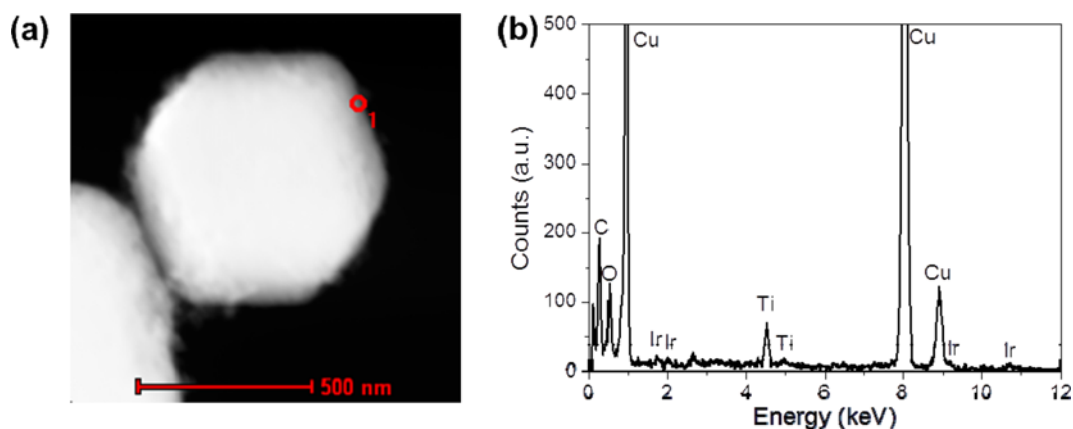
Fig. 2. (a) TEM-HAADF image of a TiIrO$_X$-coated Cu$_2$O particle. (b) EDX spectra from the region marked as spot 1 in (a).
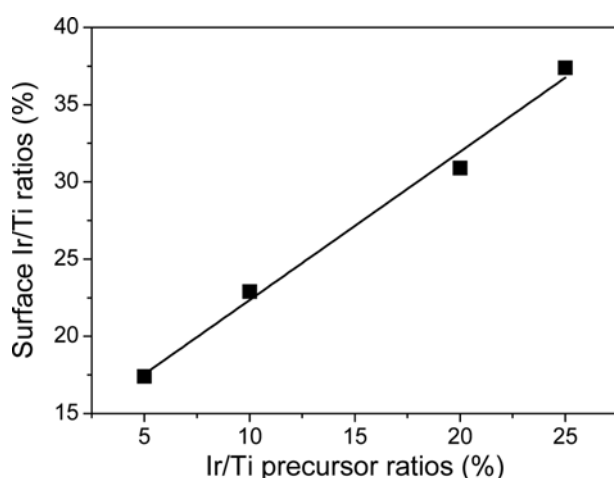

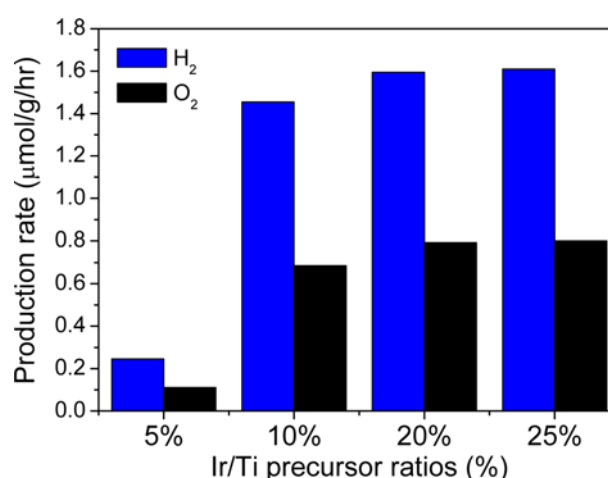**Fig. 3. The Ir/Ti precursor ratios versus surface Ir/Ti ratios measured by XPS.**

Fig. 4. Hydrogen and oxygen production rates from the TiIrO$_X$-coated Cu$_2$O particles with different Ir/Ti precursor ratios for photocatalytic water splitting.

and 25 mol%) were tested. After the coating step, the surface compositions were determined by X-ray photoelectron spectroscopy. As the Ir/Ti precursor ratio increased, the surface Ir/Ti ratio linearly increased, as can be observed in Fig. 3. The Ir species were well included in the overlayers.

These samples were applied as the photocatalyst for the water splitting reaction. The production of hydrogen and oxygen was measured for each sample. The experiments were conducted by dispersing 0.1 g of the catalyst in 100 ml of water, which was then irradiated by a 300 W Xe lamp for 24 h. Without a sacrificial agent, the overall water splitting was expected to follow a 2 : 1 hydrogen and oxygen production ratio. When 5, 10, 20, 25%-TiIrO$_X$/Cu$_2$O particles were used for the photocatalytic water splitting, the H$_2$ and O$_2$ production rates were obtained and are shown in Fig. 4. All of the samples had an H$_2$/O$_2$ production ratio of approximately 2 : 1. These results indicate that the TiIrO$_X$ overlayers prevented photocorrosion and helped with the overall water splitting. Without the coating, the holes would be consumed to produce CuO from Cu$_2$O surface with less O$_2$ production. As the Ir/Ti ratio increased, more H$_2$ and O$_2$ were produced. The 5%-TiIrO$_X$/Cu$_2$O showed poor activity. At a low Ir composition, there might not have been enough iridium

oxide channels that could have acted as hole pathways. When the Ir/Ti ratio was higher than 20%, the production rate did not undergo a further increase. Therefore, the 20%-TiIrO$_X$/Cu$_2$O was chosen in the optimization of the coating process.

The amount of water added in the synthesis of the coating was also an important factor in the optimization of the overlayer. Different amounts of water (120, 144, 168, and 200 µl) were added. These TiIrO$_X$/Cu$_2$O particles were applied in the water splitting reactions. The samples to which more water was added had a higher H$_2$ and O$_2$ production rate. However, the production rate did not further increase when the water amount was greater than 168 µl. Too much amount of water hindered the formation of conformal coating on Cu$_2$O particles. Therefore, the 168 µl-TiIrO$_X$/Cu$_2$O was chosen in the optimization of the coating process.

The different amounts of water created different Ir species in the TiIrO$_X$ layer. The oxidation state of Ir species was analyzed by XPS Ir 4f peak deconvolution (Fig. 5). The 4f$_{7/2}$ and 4f$_{5/2}$ doublet for each species was constrained to having 4 : 3 peak area ratios, equal full width at half maximum (FWHM) values, and a peak separation of 2.93 eV. There were two Ir 4f$_{7/2}$ peaks, which indicated
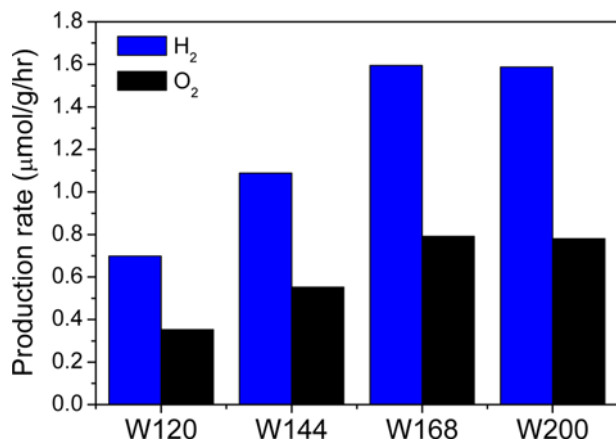
Fig. 5. Hydrogen and oxygen production rates for the TiIrO$_X$-coated Cu$_2$O synthesized with 120 μl (W120), 144 μl (W144), 168 μl (W168), and 200 μl (W200) of water.

Fig. 7. Hydrogen and oxygen production rates from the TiIrO$_x$-coated Cu$_2$O particles produced with different synthesis times for coating step.

the presence of IrO$_2$ (~61.4 eV) and IrCl$_3$ (~62.5 eV). The IrO$_2$ fraction, which was determined by the IrO$_2$ peak area divided by the areas of all of the Ir species, was 44.8% for 120 μl-TiIrO$_X$/Cu$_2$O, 60.5% for 144 μl-TiIrO$_X$/Cu$_2$O, and 94.5% for 168μl-TiIrO$_X$/Cu$_2$O. This indicated that the water induced the conversion of IrCl$_3$ into IrO$_2$. When the amount of water was 168 μl, most of the Ir precursor became IrO$_2$, which is the reason for the highest performance. No further improvement was observed by the increase in the amount of water added. These results indicate that the formation of IrO$_2$, which acted as hole channels in the TiIrO$_X$ overlayer, was essential for efficient water splitting.

The synthesis time for the coating also affected the photocatalytic water splitting reaction (Fig. 7). As the coating time increased, the H$_2$ and O$_2$ production rates increased. When the coating time was longer than 3 h, there was no significant enhancement of the H$_2$ and O$_2$ production rates.

TEM images of TiIrO$_X$-coated Cu$_2$O particles with different synthesis times for coating are presented in Fig. 8. As the synthesis time increased, the thickness of the TiIrO$_X$ overlayer increased. When the coating time was too short (0.5 h), the overlayer was thin and some regions were not coated. When the coating time was longer than 1 h, the overlayer was well coated. The thicker TiIrO$_X$ coat-
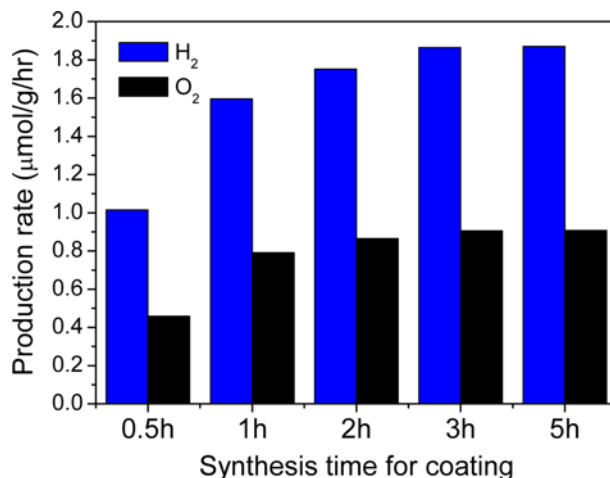
ing that was created with a longer time (3 h) caused some crystallization during the annealing process at 210 °C. The H$_2$ and O$_2$ production rates increased with the thickness of the overlayer. The crystallization might improve the quality of electron and hole channels with better transfer. But a synthesis time longer than 3 h presented no more improvement.

CONCLUSIONS

A TiIrO$_X$ overlayer was coated onto Cu$_2$O particles under various coating conditions. Each TiIrO$_X$/Cu$_2$O particle was used as a photocatalyst for the overall water splitting reaction. The ratio of Ir/Ti precursors presented a linear relation with the surface Ir/Ti ratio of the synthesized catalysts. When the surface Ir/Ti ratio increased, the H$_2$ and O$_2$ production rates increased. When more water was added during the coating process, more IrO$_2$ was formed at the surface with higher H$_2$ and O$_2$ production rate. This is important in the formation of efficient hole pathways in the TiIrO$_X$ overlayer. Otherwise, Cu$_2$O would be easily changed to CuO by the holes. The thickness of the overlayer is also important. The thickness of the coating increased with an increase in the synthesis time to form
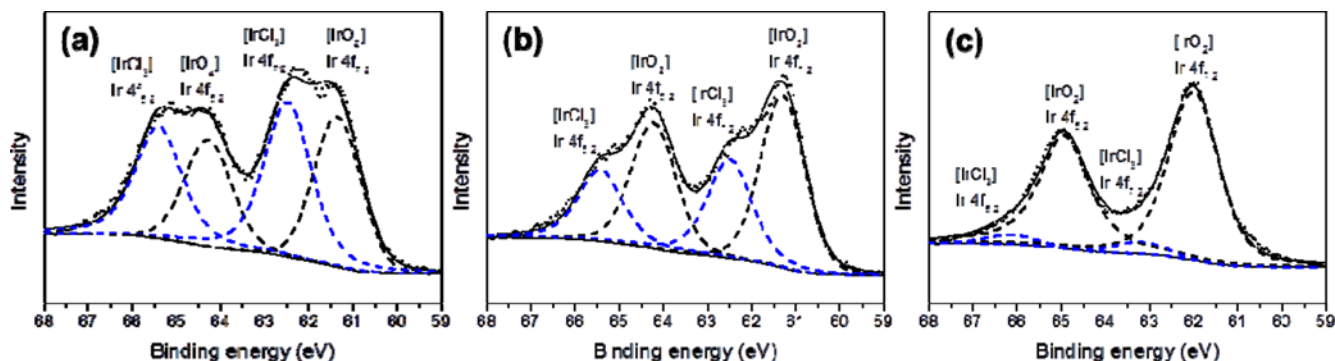

Fig. 6. XPS Ir 4f data with peak deconvolutions for the TiIrO$_X$-coated Cu$_2$O with (a) 120 μl, (b) 144 μl, and (c) 168 μl of water added. Black dashed lines represents IrO$_2$ and blue dashed line represents IrCl$_3$.
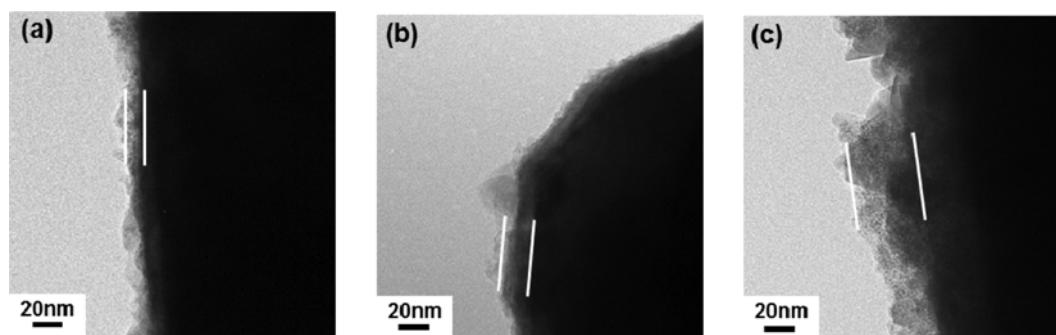
Fig. 8. TEM images of the TiIrO$_X$-coated Cu$_2$O with different synthesis times for coating. (a) 0.5 h, (b) 1 h and (c) 3 h. White bars indicate a coating layer.

the coating. As the coating layer became thicker, the activity increased. The highest H$_2$ and O$_2$ production rates occurred when the surface Ir/Ti ratio was 20%, the water addition in the coating formation was 168 μl, and the coating time was 3 h. The optimized TiIrO$_X$ overlayer can be applied for photocatalysts to enhance the stability and the activity during photoreactions.

ACKNOWLEDGEMENT

REFERENCES

1. R. Abe, *J. Photochem. Photobio. C - Photochem. Rev.*, **11**, 179 (2010).
2. K. Maeda, *J. Photochem. Photobiol. C-Photochem. Rev.*, **12**, 237 (2011).
3. A. Fujishima and K. Honda, *Nature*, **238**, 37 (1972).
4. X. B. Chen, S. H. Shen, L. J. Guo and S. S. Mao, *Chem. Rev.*, **110**, 6503 (2010).
5. W. H. Hung, T. M. Chien and C. M. Tseng, *J. Phys. Chem. C*, **118**, 12676 (2014).
6. H. Kato, K. Asakura and A. Kudo, *J. Am. Chem. Soc.*, **125**, 3082 (2003).
7. K. Yamaguti and S. Sato, *J. Chem. Soc., Faraday Trans. I*, **81**, 1237 (1985).
8. G. N. Schrauzer and T. D. Guth, *J. Am. Chem. Soc.*, **99**, 7189 (1977).
9. T. Takata and K. Domen, *J. Phys. Chem. C*, **113**, 19386 (2009).
10. J. Kim, D. Hwang, S. Bae, Y. Kim and J. Lee, *Korean J. Chem. Eng.*, **18**, 941 (2001).
11. O. Diwald, T. L. Thompson, T. Zubkov, E. G. Goralski, S. D. Walck and J. T. Yates, *J. Phys. Chem. B*, **108**, 6004 (2004).
12. T. Ohno, M. Akiyoshi, T. Umebayashi, K. Asai, T. Mitsui and M. Matsumura, *Appl. Catal. A-Gen.*, **265**, 115 (2004).
13. A. Kudo and Y. Miseki, *Chem. Soc. Rev.*, **38**, 253 (2009).
14. K. Kalyanasundaram, E. Borgarello, D. Duonghong and M. Gratzel, *Angew. Chem. Int. Ed.*, **20**, 987 (1981).
15. H. Matsumoto, T. Sakata, H. Mori and H. Yoneyama, *J. Phys. Chem.*, **100**, 13781 (1996).
16. E. Hong, J. Kim, S. Yu and J. Kim, *Korean J. Chem. Eng.*, **28**, 1684 (2011).
17. H. B. Fu, T. G. Xu, S. B. Zhu and Y. F. Zhu, *Environ. Sci. Technol.*, **42**, 8064 (2008).
18. L. L. Ma, H. Z. Sun, Y. G. Zhang, Y. L. Lin, J. L. Li, K. W. Y. Yu, Y. Yu, M. Tan and J. B. Wang, *Nanotechnology*, **19** (2008).
19. X. L. Nie, S. H. Wei and S. B. Zhang, *Phys. Rev. B*, **65** (2002).
20. Y. Jiang, H. K. Yuan and H. Chen, *Phys. Chem. Chem. Phys.*, **17**, 630 (2015).
21. X. G. Yan, L. Xu, W. Q. Huang, G. F. Huang, Z. M. Yang, S. Q. Zhan and J. P. Long, *Mater. Sci. Semicond. Process.*, **23**, 34 (2014).
22. P. E. de Jongh, D. Vanmaekelbergh and J. J. Kelly, *J. Electrochem. Soc.*, **147**, 486 (2000).
23. M. Hara, T. Kondo, M. Komoda, S. Ikeda, K. Shinohara, A. Tanaka, J. N. Kondo and K. Domen, *Chem. Commun.*, 357 (1998).
24. M. Pourbaix, *Atlas of electrochemical equilibria in aqueous solutions*, National Association of Corrosion Engineers, Houston, Texas (1974).
25. S. Kakuta and T. Abe, *Electrochem. Solid State Lett.*, **12**, P1 (2009).
26. A. Paracchino, N. Mathews, T. Hisatomi, M. Stefik, S. D. Tilley and M. Gratzel, *Energy Environ. Sci.*, **5**, 8673 (2012).
27. C. M. Wang and C. Y. Wang, *J. Nanophoton.*, **8** (2014).
28. L. I. Bendavid and E. A. Carter, *J. Phys. Chem. B*, **117**, 15750 (2013).
29. Y. Kwon, A. Soon, H. Han and H. Lee, *J. Mater. Chem. A*, **3**, 156 (2015).
30. X. D. Liang, L. Gao, S. W. Yang, and J. Sun, *Adv. Mater.*, **21**, 2068 (2009).